Elastic and inelastic scattering in quantum dots in the Coulomb-blockade regime

Gerhard Klimeck,* Roger Lake,† and Supriyo Datta
Purdue University, School of Electrical Engineering, West Lafayette, Indiana 47907-1285

Garnett W. Bryant
U.S. Army Research Laboratory, Microphotonic Devices Branch, Adelphi, Maryland 20783-1197
(Received 28 March 1994)

Starting from a rate-equation model proposed by Beenakker, we calculate current-voltage characteristics for symmetric and asymmetric vertical quantum dots. We include up to 26 electrons and show how single-electron charge interaction, inelastic scattering, and nonadiabatic subband mixing can enhance the valley current significantly by opening new conduction channels. Subband mixing is the dominant mechanism increasing the valley current in both symmetric and asymmetric quantum dots. Single-electron charging is important in asymmetric structures but relatively weak in symmetric structures. Effects of inelastic scattering within the quantum dot are dramatic for asymmetric structures, but negligible in symmetric structures.

I. INTRODUCTION

Large cross section double barrier resonant tunneling diodes (DBRTD's) have been extensively[1-3] studied and the quantization of the single-electron states in the film growth direction has been shown to be crucial in the understanding of this quantum device. Charge accumulation[4,5] and inelastic scattering[6,7] have also been shown to modify the device behavior significantly and these interactions have been successfully treated with effective potentials in a single-electron picture.

In small cross section resonant tunneling diodes electrons are confined in all three dimensions.[8-12] This confinement of a few electrons has two consequences: (1) the electronic state spectrum will be discrete and (2) the usual effective potential treatment of electron-electron interactions becomes invalid and it is necessary to go beyond the single-particle picture in order to account for electronic correlations. Single-electron correlations have been observed[8,9] in very asymmetric structures in a bias direction where the collector barrier is thicker and/or higher than the emitter barrier. This configuration corresponds to the one in which intrinsic bistability due to charge accumulation has been observed in large cross section DBRTD's.[4] In the other bias direction,[8] there is no charge accumulation at all and a very rich resonance spectrum can be observed. Beenakker[13] and Averin et al.[14] have put forward similar rate-equation models that include single-electron charge correlation and zero-dimensional (0D)-states in the quantum dot.

Lateral confinement not only alters the single-particle electronic states of the quantum dot, but also quantizes the contact states into waveguidelike subbands. The lateral confinement is determined by the charge depletion width at the lateral boundaries. The charge depletion, and hence the lateral confinement, and the lateral energy quantization change with the changing doping level

along the growth axis of the structure. The role of the transverse subbands in the leads on high bias transport has been analyzed theoretically for symmetric quantum dots using the assumption of negligible charge accumulation with a single-particle transmission coefficient approach.[11,15-18] It has been found by comparison to experimental results[10,11] that effects due to subbands in the emitter leading to the quantum dot are significant in high bias I-V characteristics. In particular it was shown that nonadiabatic transport processes, which couple lead subbands to quantum dot states of different lateral quantum numbers, cause additional resonance features in the valley current region.[16,11]

The treatments including single-electron charging and elastic and inelastic scattering[13,14] do not consider effects due to subband mixing. The treatments of subband mixing[15-17] do not include single-electron charging and inelastic scattering. In this work we combine the two treatments to provide a comprehensive model that includes subband mixing, single-electron charging, and inelastic scattering for arbitrary bias. This allows us to address the following questions:

(1) Can Coulomb charge correlation play a role in symmetric structures? Symmetric quantum dots (whose emitter and collector barrier heights are equal in flat-band condition) are expected to have little charge accumulation in either bias direction because the applied bias effectively lowers the collector barrier height relative to the emitter barrier height and the rate of outflow to the collector is larger than the rate of inflow into the quantum dot from the emitter. The transport is expected to be mostly determined by the single-particle states and indeed a rich spectrum of resonance energies has been found experimentally.[10-12]

(2) Is subband mixing as important in very asymmetric structures as it is in symmetric structures? One may argue that this may not be the case since the thick collec-

tor barrier governs the transport through an asymmetric structure and modifications due to coupling at the emitter will be negligible.

(3) How important is the inelastic scattering in high bias transport through quantum dots? Can high bias I-V characteristics be used to indicate the rate of energy relaxation in the dot? Averin et al.[14] assumed in their high bias calculation that the inelastic scattering is strong $(1/\tau \gg \Gamma^L + \Gamma^R)$ such that the electron distribution in the quantum dot is thermalized. Tunneling rates through single barriers may vary in a wide range from 10^9 to 10^{13} $1/s$ depending on the height and thickness of the barriers. Inelastic scattering rates in quantum dots have been estimated[19] to be in the same range. Direct measurements of intraband relaxation rates in quantum dots, for example, by optical methods appear to be very difficult and we are not aware of any such measurements. With a thorough analysis of the differences between the limits[20,21] of no inelastic scattering $1/\tau = 0$ and strong inelastic scattering $1/\tau \gg \Gamma^{L(R)}$, we will try to shed light on the effects of strong and weak electron phonon interaction in the quantum dots on the high bias I-V characteristic.

In Sec. II A we first illustrate the many-body rate equation approach for the case of two states in the quantum dot. We then describe the model for subband mixing (Sec. II B) and explain our numerically efficient setup of the rate equations in multiple degenerate states (Sec. II C). In Sec. III we evaluate the transport properties through two different quantum dots, symmetric and asymmetric, and address the questions stated above. We have deferred the details of the mathematical formulation to the Appendix.

II. MODEL

We are interested in modeling high bias transport through a central confined system with interacting elec-
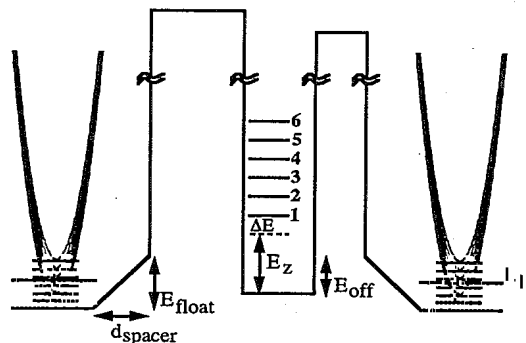

FIG. 1. Conduction band profile of a single quantum dot. Subband energy spacing in the leads is 10 meV and single-particle state energy spacing in the quantum dot is 15 meV. The Fermi energy in the leads is 38 meV (three subbands are occupied). The conduction band in the quantum dot and barriers is raised by $E_{\text{float}} = 50$ meV due to charge depletion. The quantum dot is assumed to be $In_xGa_{1-x}As$ with a conduction band offset of $E_{\text{off}} = -50$ meV. The thicknesses of the spacer layers and the quantum well are 50 and 60 Å, respectively. The longitudinal energy quantization E_z is 60 meV. The temperature is $T = 0.9$ K, corresponding to $k_bT = 0.08$ meV. Barrier thicknesses and Al fractions vary for the simulated symmetric and asymmetric structures.

trons. We are following Beenakker[13] in the modeling of high bias transport using rate equations where the many-body states in the quantum dot are coupled to adjacent leads via sequential, single-electron tunneling. The states in a quantum dot (see Fig. 1) may be a complicated superposition of single-electron states.[22-27] The assumption of constant charging energy is used to construct the many-body states in the quantum dot easily. The limitations of this ansatz are discussed in the Appendix. The complicated task in this problem is to calculate the coupling to the leads and to solve for the nonequilibrium occupation probabilities of all many-body states in the quantum dot.

A. Rate equations

To illustrate the rate-equation setup in the configuration space notation we consider a limited system of only two single-particle states (Fig. 2). There are four possible configurations $\{n_1, n_2\}$ of electrons in the quantum dot: $\{0,0\}$, $\{1,0\}$, $\{0,1\}$, and $\{1,1\}$. The respective eigenenergies $E_{\{n_1,n_2\}}$ of these four states are 0, E_1, E_2, and $E_1 + E_2 + U$, where U indicates the modification of the eigenenergy due to electron-electron charge interaction. Figure 2(a) depicts the eigenenergy spectrum of this simple many-body system and its associated transition energies.

The transitions between these many-body states are due to the tunneling to the adjacent leads as indicated in Fig. 2(b). The excited state $\{0,1\}$, for example, is coupled to three other states via five different processes. The configuration $\{0,1\}$ can be destroyed by (1) tunneling of a second electron into state n_1 to create the $\{1,1\}$ state at a rate of $\Gamma_3 f_3$, (2) tunneling of the n_2 electron into the leads to create the $\{0,0\}$ state at a rate $\Gamma_2(1-f_2)$, and (3) relaxation to the $\{1,0\}$ configuration at a rate $1/\tau$. The configuration $\{0,1\}$ can be created by (1) tunneling of an electron into state n_2 from the $\{0,0\}$ configuration at a rate $\Gamma_2 f_2$ and (2) tunneling of an electron out of the n_1 state from the $\{1,1\}$ configuration at a rate of $\Gamma_3(1-f_3)$. For legibility we have abbreviated, for exam-
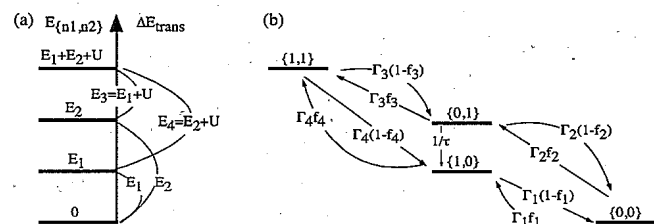

FIG. 2. Interacting two-particle system. (a) Eigenenergy spectrum and transition energies. (b) Configurations $\{n_1, n_2\}$ ordered vertically by their corresponding eigenenergy in (a). Coupling between configurations depends on transition rates Γ, availability of initial (f), final $(1-f)$ states, and the necessary transition energy (subscripts 1-4). $1/\tau$ indicates the intradot relaxation between configurations of constant number of particles.

ple, $\Gamma_2 f_2 = \Gamma_2^L f_2^L + \Gamma_2^R f_2^R$, where $\Gamma_2^{L(R)}$ is the energy and mode dependent single barrier tunneling rate through the left (right) barrier. $f_2^{L(R)}$ is the probability of finding an electron in the left (right) lead, which provides the correct transition energy. Similarly we have abbreviated $\Gamma_3(1-f_3) = \Gamma_3^L(1-f_3^L) + \Gamma_3^R(1-f_3^R)$, where $(1-f_3^{L(R)})$ is the probability of finding an available state in the left (right) lead. All other transitions with changing numbers of electrons are similar, where we have indexed Γ's and f's by their appropriate transition energies $E_1, E_2, E_3 = E_1 + U$ and $E_4 = E_2 + U$. Each configuration $\{n_1, n_2\}$ has an associated steady state occupation probability $P(\{n_1, n_2\})$, which is a function of the coupling to the leads and the quantum dot relaxation time. This picture described here is identical to the one used by Beenakker[13] to model linear response, except for the finite relaxation rate[20] $1/\tau$. We reformulate the rate equations to make the treatment of a significant number of states numerically feasible and solve it for high bias.

The equations we actually solve provide no additional physical insight to Fig. 2 and their discussion has been deferred to the Appendix. Effects due to non-adiabatic transport enter our treatment via the tunneling rates Γ, which will be discussed in the next subsection.

B. Subband mixing: The model

We use the theory of multichannel quantum dot tunneling which we developed and employed previously to study resonant tunneling through single dots with abrupt connections,[15-17] through dots with tapered connections,[17] and through coupled quantum dots.[28] We assume that the quantum dot nanostructure is a cylinder which is divided into separate regions for the emitter, the barrier between the emitter and the dot, the dot, the other barrier, and the collector. We assume that the lateral confinement potential in each region is parabolic. In each region the electron effective mass, lateral confinement potential, and the conduction band edge are locally constant. However, these parameters can change from region to region. To calculate the transmission coefficient for single barrier tunneling into (out of) the quantum dot, we propagate an electron incident from the emitter (collector) through the connection, across the barrier, and into the dot. Wave function boundary conditions are satisfied at each interface between adjacent regions. Details are given in Refs. 15 and 17.

Mode mixing is determined by how the lateral confinement potential changes where the leads connect to the dot. In previous work[15-17,28] we have found that mode mixing is qualitatively the same for abrupt or tapered connections and we assume here that the connections are abrupt to simplify the calculations. The overlaps

$$\langle l, m | r, q \rangle = \int dx \, dy \, \phi_{lm}^* \, \phi_{rq} \qquad (1)$$

between lateral states $\phi_{j,q}(x, y)$ on adjacent sides of an interface, $j = l$ (left) or $j = r$ (right), with a set of lateral quantum numbers q, determine which lateral modes

mix at an interface and how strong the mixing will be. If confinement is the same on both sides of the interface, then $\langle l, m | r, q \rangle = \delta_{m,q}$ and tunneling is a single-channel process. When the confinement is different in two adjacent regions, then lateral mode mixing at the interface is possible.

When the quantum structure is cylindrically symmetric, as in a vertical quantum dot structure with parabolic confining potentials, the lateral modes in different regions can mix only if the modes have the same lateral $(x-y)$ parity. There are four independent sets of coupled channels [Fig. 3(a)] with even-even, odd-even, even-odd, and odd-odd parity. We include the ground states $(0,0)$, $(1,0)$, $(0,1)$, and $(1,1)$ and the first three excited states for the first three parity groups. We have to leave out the $(3,1)$, $(1,3)$, and $(3,3)$ states due to numerical limitations (see Sec. II C). The resulting single-particle spectrum is depicted in Fig. 3(b). Note that each of these indicated states is spin degenerate.

For our simple model the overlap matrix for $x(y)$ motion is 2×2. To conserve probability, the matrix must be unitary.[15] A real, unitary 2×2 matrix has the form

$$\begin{pmatrix} \beta & \gamma \\ -\gamma & \beta \end{pmatrix}.$$

where $|\gamma| = (1 - \beta^2)^{1/2}$. If we specify β_x and β_y for the x and y overlaps, the total overlap matrix for the four coupled modes can be determined. For cylindrical structures $\beta_x = \beta_y = \beta$. Thus a single parameter determines the overlap matrix for a particular interface.

The strength β for the lateral mode coupling is determined by the overlap between lateral states in adjacent regions. If the confining potentials are parabolic, then the overlaps can be determined analytically. Even if the confining potential is not exactly parabolic, the parabolic approximation should give a good qualitative estimate for the overlaps if the correct effective masses and lateral level spacings are used to model the parabolic
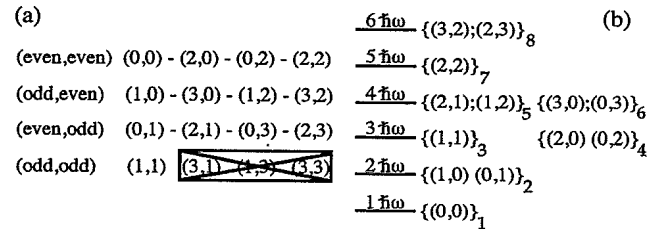

FIG. 3. (a) Subset of 16 lateral single-particle states (n_x, n_y) composed of four allowed quantum numbers in each dimension. Only states with the same x and y parity can couple to each other, as indicated by horizontal odering and connections with dashes. States $(3,1)$, $(1,3)$, and $(3,3)$ are excluded in our calculation for reasons of numerical complexity. (b) Lateral single-particle eigenenergy spectrum. Each quantum state (n_x, n_y) is doubly spin degenerate. Grouping in curly brackets $\{\ \}_i$ indicates degeneracy and equivalent coupling to the leads; i.e., states in one group i are equally likely occupied.

potentials. Estimates of β have been made for abrupt constrictions.[15] For parameters appropriate for the quantum dot nanostructures, $\beta > 0.6$. In these calculations, we use β as a parameter which we adjust in this range to test the effects of mode mixing.

The tunneling rates $\Gamma^{L(R)}$ are calculated for the barrier under bias. They depend on the modes and their mixing as described above, and they depend on the longitudinal energy through the barrier transmission coefficient and the attempt frequency in the well.[29,30] The longitudinal energy dependence goes as $(E - \epsilon_m)^{1/2}$, where E is the total energy and ϵ_m is the transverse energy of mode m. Averin et al.[14] included only the energy dependence of the tunneling rate through the emitter. The energy dependence of the tunneling rate through the collector is equally important when subband mixing is included and is especially important for asymmetric structures where the current is largely determined by the escape rate through the collector barrier.

C. Implementation of rate equations

The rate equations as they were put forward by Beenakker[13] use a notation that indicates the occupation and vacancy in a Slater determinant state by a 1 and a 0, respectively. The solution of the rate equations becomes exponentially complex with an increasing number of basis states, since 2^{2p} different configurations exist for the maximum number of p spin-degenerate single-particle states in the quantum dot, resulting in a set of 2^{2p} coupled equations ($2^{2p} \times 2^{2p}$ matrix). The problem simplifies dramatically if certain assumptions about the occupation of states can be made. Beenakker[13] has solved these coupled equations in the limit of linear response for the analysis of periodic conductance oscillations, where the states are assumed to be in local equilibrium.

In high bias, however, the electron distribution is driven far away from its equilibrium value. Averin et al.[14] have considered, in their high bias calculation, the case of rapid thermalization (i.e., strong inelastic scattering) in the quantum dot where the total number of electrons in the dot at high bias can be far away from its equilibrium value; however, the electron distribution in the subset of constant number of electrons N is given by its equilibrium value. This assumption of rapid thermalization in the quantum dot simplifies the necessary calculations significantly since only the nonequilibrium number of electrons in the dot needs to be calculated. The problem reduces from 2^{2p} to $2p$ unknowns. We make this assumption of rapid thermalization in our numerical work when we include inelastic scattering. However, in the elastic case we solve for the probability of relaxation of all configurations which is numerically a formidable task.

Figure 3(b) indicates the structure of the single-electron quantum states that we are simulating. Altogether we are considering 13 spin-degenerate states. The number of all possible configurations of these 26 quantum numbers in terms of an occupation number notation in a limited single-particle basis set of 13 states is

$2^{26} \approx 6.7 \times 10^7$. The setup for a solution for all of the occupation probabilities would therefore result in a matrix of dimension $2^{26} \times 2^{26}$. However, many of the lateral states are degenerate in energy and have equivalent coupling to the leads. This degeneracy can be used to reduce the number of equations that need to be solved.

To illustrate this degeneracy of states let us consider single-particle lateral states characterized by two lateral quantum numbers (n_x, n_y). Figure 3(b) shows the single-particle spectrum grouped by degenerate states and complementary parity. Each element in one group of states, e.g., $\{(1,0);(0,1)\}_2$ is coupled to other single-particle states, e.g., $(odd, even) - (1,0) - (3,0) - (1,2) - (3,2)$ and $(even, odd) - (0,1) - (2,1) - (0,3) - (2,3)$, as indicated in Fig. 3(a). These coupled single-particle states form again distinct groups $\{(2,1);(1,2)\}_5$, $\{(3,0);(0,3)\}_6$, and $\{(3,2);(2,3)\}_8$. Since the elements in the groups are degenerate and the coupling of elements in different groups is determined by the group label, each of the single-particle states in one group have the same probability to be occupied. Instead of calculating 26 occupation probabilities (13 states $\times$ 2 spins) we only need to calculate 8 probabilities.

This grouping of states can also be utilized for the many-body state notation as explained in the Appendix. We can assume our system to have five four-fold degenerate and three two-fold degenerate states with a configuration space of $5^5 \times 3^3 = 84\,375$. We can solve a system of equations of this dimension[31,32] using iterative methods,[33] if we can provide a "good" guess for the solution. We defer the report of the rate equations, which utilize the degeneracies discussed above, and how we obtain an initial guess for the solution to the Appendix.

III. NUMERICAL RESULTS

In this section we present our results obtained for a multielectron quantum dot system under high bias. We consider two example systems here: an asymmetric and a symmetric structure in which we analyze the effects of nonadiabatic transport, electron-electron charging, and inelastic scattering.

A. Example device

The device we consider here is an undoped $Al_xGa_{1-x}As$ double barrier resonant tunneling structure (Fig. 1), which is sandwiched between lightly doped spacer layers and heavily doped contact layers. The transverse confinement changes in the longitudinal dimension due to the change of doping and the associated charge depletion along the growth axis of the diode. The single-particle energy spacing in the quantum dot, barriers, and leads is assumed to be 15, 16, and 10 meV, respectively. A Fermi energy of 38 meV populates the three lowest subbands in the leads. The conduction band floats up in the central region of the device due to the lack of doping $V_{float} = 50$ meV. The well region is assumed to be $In_xGa_{1-x}As$ with a conduction band offset of $E_{off} = -50$ meV and thick-

ness of 60 Å similar to the Reed[10] structure. We have estimated the energy quantization in the longitudinal direction to be 60 meV and 245 meV for the first two states with our Green's function simulator QUEST.[34] Since the energy separation of these two longitudinal states is much larger than the assumed lateral state quantization, we will neglect the second longitudinal state completely.

We assume that the single-particle state separations, $\Delta E = 15$ meV are larger than the charging energy, $U = 1.5$ meV. This allows us to use the simple charge interaction model (see Appendix A 3). Barrier thicknesses and Al fractions[35] are chosen such that the single-particle levels can be assumed to be sharp compared to the temperature, charging energy, and single-particle spectrum ($\Delta E, U > k_B T \gg \hbar \Gamma$) in order to use rate equations in the sequential tunneling picture.

B. Inelastic scattering, charging, and subband mixing treated independently

Let us first look at the consequences of the three phenomena (inelastic scattering, charging, and subband mixing) independently in this complicated electronic system. For these examples we consider an asymmetric structure with left/right barrier thicknesses of 105 Å/80 Å and an Al fraction of 0.35/0.30 corresponding[35] to a barrier height of 262/224 meV.

We use the calculation for elastic, adiabatic, no charge-interaction transport as baseline (thin line in Figs. 4–6) for comparison against the independent inclusions of inelastic scattering (Fig. 4), charge interaction (Fig. 5), and subband mixing (Fig. 6). The arrows marked x-y in Fig 4 indicate the voltage ranges over which subband x in the *emitter* can conduct adiabatically into quantum state y in the quantum dot. x and y correspond to subscripts indicating the groups of single electron states in
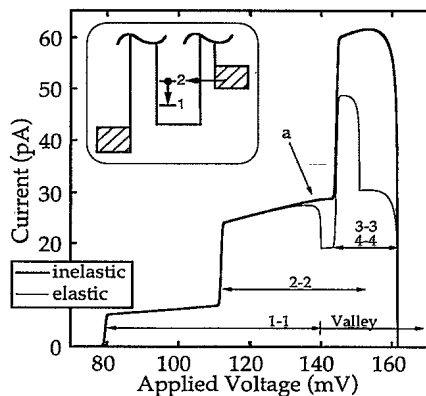

FIG. 4. *I-V* characteristic for an asymmetric structure. Effects due to thermalization (thick line) compared to the elastic, adiabatic, single-particle result. Arrows labeled 1-1, 2-2, 3-3, and 4-4 indicate the regions of allowed adiabatic, elastic subband-to-quantum-state transitions (thin line). Electron relaxation wipes out features and increases the current in the "valley current" region where channel 1 has shut off already. The inset shows a two-state model indicating vertical flow into elastically decoupled level 1.

Fig. 3(b). Without subband mixing three[36] occupied subbands in the emitter couple to their corresponding lateral states in the quantum dot and three distinct current steps are observable in the *I-V* characteristic. Note that the 3-3 transition is turning on when the 1-1 transition is already turned off due to (1) the different energy separations of the subbands in the leads (10 meV) and the single-electron states in the quantum dot (15 meV) and (2) the finite Fermi energy in the leads. We define the valley current region as the voltage region extending past the turnoff of the first transition (see Fig. 4).

The introduction of inelastic scattering in the limit of complete thermalization ($k_B T \gg \hbar / \tau \gg \Gamma$) (thick line in Fig. 4) shows an increased current due to coupling of lower lying, elastically decoupled channels. The turnoff of the 1-1 transition, for example, introduces a decrease in the current in the elastic calculation (arrow a); however, electrons tunneling into the quantum dot in a 2-2 transition can relax down to level 1 in the quantum dot (see inset in Fig. 4). Level 1 is therefore filled "from the top" via an inelastic channel. The current is increased due to this additional channel[29,30] and the turnoff feature of the 1-1 transition is wiped out. The effect of filling of a lower lying level depends strongly on ratio of the rate of outflow to the collector versus inflow from the emitter.[21,29,30] It can be shown analytically[21] for a two-state system that a large asymmetry $\Gamma^L \ll \Gamma^R$ (with the bias such that the electron flow is from right to left), the current effectively doubles to a two-channel result. For $\Gamma^R = \Gamma^L$ the current enhancement due to inelastic scattering is 60%. For $\Gamma^L \gg \Gamma^R$, the current enhancement is small and the current remains basically carried by one channel.

Figure 5 shows the effects of single-electron charging in the elastic limit ($1/\tau = 0$). Steps reflecting the charging energy scale U are introduced. The spin degeneracy of the first level [$1\hbar\omega$ in Fig. 3(b)] is broken[9] (arrow 1). The step from the single-particle turnon (arrow 2) consisting of four degenerate states [$2\hbar\omega$ in Fig. 3(b)] is broken into four steps starting at arrow 3. A factor of 2 enhancement of the total current at a bias where six electrons are in the quantum dot ($\langle N \rangle \lesssim 6$) at arrow 4 compared to the current level at arrow 2 where we also have six electrons in the quantum dot ($\langle N \rangle \lesssim 6$) is due to an increased transparency of the collector barrier in the presence of charging. Since total energy is conserved in the tunneling process, an increased energy due to charging allows coupling to higher energy states in the collector and therefore increases the collector barrier transparency.

Notice that there is a hint of a step at about 120 meV which is due to the addition of a single-particle channel [see Fig. 3(b)] into the quantum dot. In the asymmetric structure the amplitude of the current is mostly determined by the (almost) quantized number of particles in the quantum dot and the tunneling rate out of the quantum dot as long as one single-particle channel into the dot is available. The addition of an entry channel given the presence of some other entry channels does therefore not increase the current strongly.[21] By the same argument we do not find a characteristic turnon due to the third single-particle level [$3\hbar\omega$ in Fig. 3(b)] in the case of

charge correlation compared to the single-particle result (arrow 5).[37]

The current calculated including charge correlation does not turn off sharply as single-particle state 1 is turned off. On the contrary, the valley current is increased strongly by charge correlation. The origin of such current increase can be understood in a simple two-state model indicated in the inset of Fig. 5. Given a bias where state 1 is pulled under the conduction band edge of the emitter, only state 2 appears to be available to be tunneled into in a single-electron picture. However, an electron "residing" in state 2 changes the single-particle excitation spectrum significantly and may "lift" unfilled level 1 into an energy range in which tunneling is allowed. If state 2 is occupied long enough, state 1 will fill and two electrons are "waiting" to tunnel to the collector, corresponding to two transmission channels. We can show analytically[21] that the current enhancement for the inclusion of single-electron charging in the two-state example at this bias is $\delta = \frac{I_{U\neq0}-I_{U=0}}{I_{U=0}} = \frac{2\Gamma_L\Gamma_R+\Gamma_R^2}{2\Gamma_L^2+2\Gamma_L\Gamma_R+\Gamma_R^2}$. Given an asymmetry $\Gamma_L \ll \Gamma_R$ (collector barrier larger and/or thicker than emitter barrier), we have an enhancement $\delta \approx 1-2\left(\frac{\Gamma_L}{\Gamma_R}\right)^2 \to 1 = 100\%$ corresponding to two channels. Even for $\Gamma_R = \Gamma_L$, we have an enhancement $\delta = \frac{3}{5} = 60\%$ over the noninteracting result. The current enhancement given very leaky conditions $\Gamma_L \gg \Gamma_R$ is $\delta \approx \frac{\Gamma_R}{\Gamma_L} \to 0$.

Figure 6 depicts the simulation result including weak subband mixing of strength $\beta = 0.95$. The labels x-y indicate the additional channels due to tunneling from subband x in the emitter to state y in the quantum dot as with the corresponding labels (1 − 8) in Fig. 3(b). The inclusion of subband mixing extends the voltage region of conductance significantly and the I-V characteristic exhibits an additional structure[32] due to the modes in the leads and quantum dot. Current conservation demands
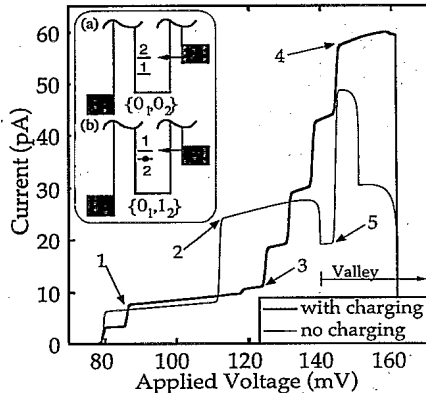
FIG. 5. I-V characteristic for an asymmetric structure. Effects due electron charge correlation (thick line) compared to the elastic, adiabatic, single-particle result (thin line). State degeneracy is broken (arrows 1 and 3) and the turnon of the second single-particle level is impeded (arrow 2). The current is increased in the valley current region (arrow 4). The inset shows a physical picture of the enhanced valley current due to electron-electron correlation. There is no explicit turnon of level 3 (arrow 5). The underlying single-particle spectrum cannot be identified.
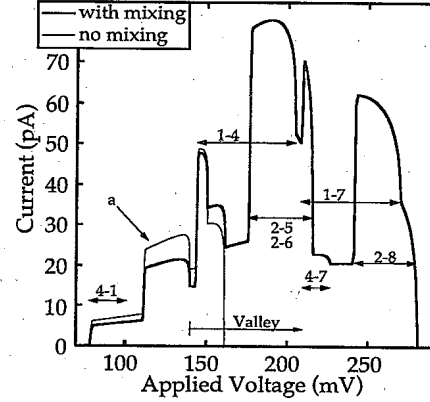
FIG. 6. I-V characteristic for an asymmetric structure. Effects due to subband mixing (thick line) are compared to the elastic, adiabatic, single-particle result (thin line). Subband mixing increases the voltage-region of the current flow. Features due to turnons and turnoffs of quantum states in the dot and subbands in the leads are exposed. The notation of new channels x-y is the same as in Fig. 4. The unitarity condition on the scattering matrix causes reduced current flow through direct channels (arrow a) due to the opening of other scattering channels.

that the scattering matrix which couples subbands and quantum states in the dot to be unitary (see Sec. II B). Opening new scattering channels reduces the strength of the direct channels, resulting in a smaller current contribution from the direct channels (arrow a). These calculations were performed for an asymmetric structure and they show clearly that, although the current through an asymmetric structure may be dominated by the collector barrier transmission rate, the addition of entry channels on the emitter side can increase the valley current dramatically, when the direct channels start to turn off.

In the following two subsections we will now put the three transport phenomena—(1) elastic vs thermalized transport, (2) noninteracting vs interacting transport, and (3) adiabatic vs nonadiabatic transport—together piece by piece and explain their general effects on asymmetric and symmetric structures. For the asymmetric structure we start from Averin, Korotkov, and Likharev's[14] analysis of adiabatic, thermalized transport through a charge interacting quantum dot and show how the inclusion of nonadiabatic transport phenomena and the exclusion of inelastic scattering in the quantum dot will alter the high bias I-V characteristic dramatically. For the symmetric structure we start from Bryant's[15−17] analysis of nonadiabatic transport in symmetric structures and add charge correlation and inelastic scattering.

C. Asymmetric structure

Averin et al.[14] have assumed adiabatic coupling from 1D subbands in the leads to 0D states in the quantum dot for the lowest longitudinal energy level in their high bias transport analysis. They assumed that the electrons are in the quantum dot long enough to suffer inelastic scattering processes and calculated the canonical ensemble

average. We start our analysis for asymmetric structures from this picture. However, note that in our case we assume that the Fermi energy E_F is the same order of magnitude as the subband separation ΔE such that only few subbands are occupied in the leads (Fig. 1). This assumption allows us to analyze the effects of subband mixing and corresponds to doping levels similar to the structure by Reed et al.[10] in which subband mixing is indeed important.[16,17] Another difference in our analysis is that we keep the energy dependence of the collector barrier transmission rates, which makes the collector barrier more leaky at higher biases and reduces the charge accumulation. Also we do not include effects due to bistability

FIG. 7. I-V characteristic for an asymmetric structure. We start with Averin, Korotkov, and Likharev's (Ref. 14) "picture" of inelastic, adiabatic transport with and without single-electron charging and show effects due to the inclusion of subband mixing and the exclusion of inelastic scattering. (a) Single-electron charging: Single-electron charging (thick line) introduces fine structure in the I-V characteristic and breaks single-particle state degeneracy (arrows 1 and 2). (b) Include nonadiabatic transport: Thick line in (a) is now thin. Subband mixing (thick line) increases the region of current flow. Features due to single-electron charging ($\approx 2 \times U = 3$ meV are dominant. Single-electron particle spectrum (see Fig. 6) cannot be identified. (c) Exclude inelastic scattering: Thick line in (b) is now thin. Fine structure due to the single-particle spectrum is exposed (see Fig. 6). Inset: The I-V characteristic for a reverse bias measurement where the thick barrier is now the emitter barrier. The I-V characteristic is determined by the single-particle spectrum (ΔE).

here as discussed in the Appendix.

The asymmetric double barrier structure analyzed here is the same one as considered in the previous examples. The thin line in Fig. 7(a) is the thick line in Fig. 4 given strong inelastic scattering, no charging, and no subband mixing. Now we add charging to the simulation to obtain the thick line of Fig. 7(a). This thick line of Fig. 7(a) is almost identical to the thick line of Fig. 5. Single-electron state degeneracies are broken (arrows 1 and 2) by the charge correlation and no explicit turnon of the third quantum level is visible (arrow 3) as discussed above. The fact that the two current amplitudes to the right of arrow 3 are nearly equal is coincidental.

Is subband mixing important in asymmetric structures? In Fig. 7(b) we add weak subband mixing ($\beta = 0.95$) to the result shown in Fig. 7(a) and we effectively combine the results of Figs. 4–6. Figure 6 has shown that subband mixing increases the voltage range of conductance and Fig. 5 has shown that charging increases the current in the valley current region. Both of these effects are strikingly evident in Fig. 7(b).

Does inelastic scattering play a role in asymmetric structures? Fig. 7(c) compares the I-V characteristic without inelastic scattering ($1/\tau = 0$, thick line) to the one shown in Fig. 7(b) with complete thermalization ($1/\tau \gg \Gamma$, thin line). Inelastic scattering (thin line) effectively couples lower lying quantum levels, which are not coupled elastically to the emitter lead in the valley current region.[29,30] The I-V characteristic appears as an almost monotonic staircase. The exclusion of inelastic scattering (thick line) exhibits structure due to the single-electron spectrum in the valley current region (arrows labeled ΔE) and the current is significantly reduced as levels fall under the conduction band edge of the emitter. The two limits of thermalized and elastic ($1/\tau=0$) transport give dramatically different results in forward biased asymmetric structures. A reverse bias measurement [see the inset of Fig. 7(c)] of an asymmetric structure will exhibit the single-particle spectrum only since there is no charge accumulation.[8] If single-particle features can still be found in the forward bias direction we have an indication that the relaxation in the quantum dot is not very fast compared to the collector barrier escape rate. If all the single-particle features disappear, we have an indication that the relaxation rate is large.
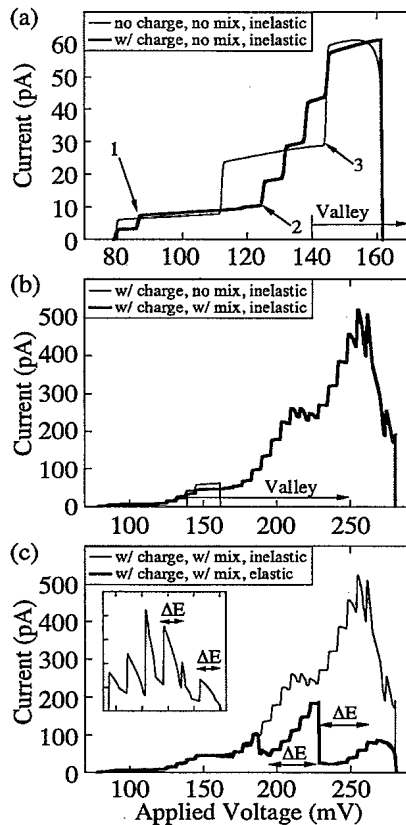
D. Symmetric structure

Is there single-electron charging? While single-particle quantum states in resonant tunneling diodes have been observed[10] in symmetric structures, there is no evidence for single-electron charging effects in such structures. The supporting argument for the missing effects due to single electron charging is that the collector barrier is effectively lowered due to the applied bias and that there is no charge accumulation to introduce effects due electron-electron interaction. However, the effect of the effective collector barrier lowering can be decreased if the barrier heights are raised. If then collector and emitter barrier transmission rates are of the same order of magnitude,

an average filling of a quantum state is $\lesssim 1/2$. This will modify the transition energy spectrum of the quantum dot and will leave an observable effect in the high bias I-V characteristic. Another requirement[13,14] $(U > k_B T \gg \hbar\Gamma)$ that is necessary for the observation of single-electron charging effects has also not been satisfied in the symmetric Reed[10] structure. We have estimated the energetic spread of the quantum states due to the coupling to the leads to be of the order of several meV, which is about the same order of magnitude of possible charging energies involved with single-electron charging. We therefore cannot expect to observe single-electron charging effects. By the choice of thick barriers we can ensure that we can satisfy the condition $U > k_B T \gg \hbar\Gamma$ for all possible transitions into and out of the quantum dot.

We analyze here the double barrier structure depicted in Fig. 1 with *equal* barrier thicknesses of 80 Å and Al fractions of 0.35 corresponding[35] to a barrier height of 262 meV. Figure 8(a) depicts an I-V characteristic that
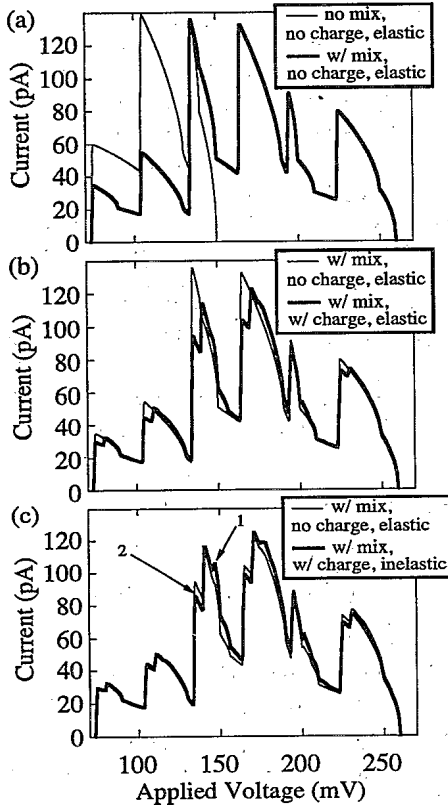

FIG. 8. I-V characteristic for a symmetric structure. We start with Bryant's (Refs. 15–17 "picture" of coherent transport with and without subband mixing and extend the model to include single-electron charging and inelastic scattering. (a) Adiabatic vs nonadiabatic transport. The voltage region of current flow is extended due to subband mixing $\beta = 0.95$ (thick line). (b) Include charging: Thick line from (a) is now thin. Electron-electron charging introduces features in the I-V characteristic even for symmetric structures. (c) Include strong inelastic scattering: Thick line from (b) is now thin. Electron relaxation in the quantum dot has only small effects on the I-V characteristic. The current is increased on the turnoff side of the peaks (arrow 1) and reduced on the turnon side (arrow 2).

Bryant[15–17] could have obtained in his analysis of coherent, elastic transport through double barrier structures. Even weak subband mixing ($\beta = 0.95$) modifies the overall I-V characteristic significantly by extending the voltage region of transport. Calculated modifications of this high bias characteristic due single-electron charge interactions are depicted in Fig. 8(b) using a charging energy of $U = 1.5$ meV. There are clearly additional steps of the energy scale of $2U$ introduced due to single-electron charging.

Does inelastic scattering play a role in symmetric structures? Figure 8(c) compares the simulations for perfectly elastic ($1/\tau = 0$) and thermalized transport in the presence of electron charge interaction and subband mixing. The thick line from Fig. 8(b) is now thin. The relative amplitudes (arrow 1) of some current peaks have changed due to the opening of new channels in the valley current. Current is slightly reduced[21] due to inelastic scattering on the rise part of the I-V characteristic (arrow 2). However, effects due to inelastic scattering in the quantum dot in the case of symmetric structures appear to be small. The two calculations for the extreme cases of elastic and thermalized transport do give slightly different results, but an experimental determination whether transport at high bias is elastic or thermalized seems infeasible.

Conclusion for symmetric structures. Our analysis shows that single-electron charging will have effects on the high bias I-V characteristic of symmetric double barrier structures, provided the barriers are thick and/or high enough. In the limit of strong confinement where $\Delta E > U$ we expect the I-V characteristic to be dominated by the single-particle spectrum. Superimposed on this spectrum we expect fine structure due to single-electron charge correlations. Devices built in this parameter range would allow the clear separation of charging and quantum effects. Effects due to inelastic scattering within the quantum dot appear to be weak. Since the assumption of thermalization in the quantum dot simplifies the problem dramatically numerically (speedup of a factor of about 10 000) and since it does include the relevant effects of charging and subband mixing now, it appears to be the solution of choice for simulations of symmetric quantum dots with large and/or thick barriers.

IV. CONCLUSIONS

We have presented numerical results which explain the roles of inelastic scattering, single-electron charge interaction and nonadiabatic coupling to the leads in the transport through a quantum dot. All three of these effects increase the valley current of the I-V characteristic compared to the noninteracting, adiabatic, single-particle analysis. We have tied two approaches together in our analysis: (1) nonadiabatic transport analysis in the elastic, no charge interaction limit[15–17] and (2) inelastic, charge interaction analysis in the adiabatic limit.[13,14] We have analyzed numerically devices where the Fermi energy is comparable to the lateral state spacing. Nonadiabatic transport increases the voltage range of transport

through symmetric and asymmetric structures and appears to be very significant if the lateral confinement is strong and only few subbands are occupied. In symmetric structures effects due to single-electron charging have not been observed experimentally. However, we show that additional steps in the *I-V* characteristic should be observable even in the case of weak charge accumulation, provided the barriers are thick and/or high enough. The inclusion of inelastic scattering within the symmetric quantum dot does not introduce significant changes in the predicted *I-V* characteristic. Transport through asymmetric structures is shown to be dominated by charge accumulation in one bias direction. Also the treatment of inelastic scattering in the forward biased asymmetric quantum dot modifies the predictions of high bias transport dramatically. Weak inelastic scattering exposes the underlying single-particle spectrum in the valley current region and the *I-V* characteristics may give insight into the strength of the inelastic scattering in the quantum dot by comparison of forward and reverse bias measurements.

Note added in proof. A. N. Korotkov brought Ref. 43 to the attention of G.K. in which the authors had compared effects due to small and large relaxation rates as discussed in this paper. The results presented in Ref. 43, however, are in a different limit of metallic granules in which the charging energy is large compared to the single-electron spectrum ($U \gg \Delta E$). In this limit certain assumptions about the occupation of the states in the granule are possible, which simplify the numerical task to calculate the occupation of the states significantly. Reference 43 concentrates on the turn-on region of the *I-V* characteristic, whereas we concentrate on the effects of elastic and inelastic scattering in the valley current region.

ACKNOWLEDGMENTS

APPENDIX: RATE EQUATIONS

In this appendix we will present the rate equations used in the numerical simulations and discuss the origin and the limitation of the constant charging model.

1. Rate equations for degenerate states

In Sec. II A we have explained, using Fig. 2, the general idea of the configuration space and the coupling between the configurations. This approach has been put forward by Beenakker[13] for the treatment of Coulomb blockade problems. In Sec. II B we discussed the single-particle spectrum that we are considering in this work and argued in Sec. II C how the multiple degeneracy of the quantum states should be exploited to reduce the number of possible many-body configurations. We use Beenakker's model for nondegenerate states and extend

it to multiple degeneracy and include a finite intradot relaxation time.

We are using a constant charging model with a single-electron charging energy[14] of

$$\tilde{U}(N) = \frac{e^2}{2C} \times N(N-1) = U \times N(N-1) \ , \quad \text{(A1)}$$

where N is the total number of electrons in the quantum dot and C is the electrostatic charge coupling of the quantum dot to the reservoirs. Beenakker assumed a charging energy of the form $\tilde{U}(N) = N^2 \frac{e^2}{2C}$, which is a good approximation for the case large N. We assume here that the first electron does *not* have a charging energy against the reservoirs.[14] The coupling to the leads is assumed to be weak enough such that the single-electron states in the quantum dot are considered to be sharp compared to the temperature $k_B T$, the single-electron energy spectrum ΔE, and charging energies U [$\Delta E, U > k_b T \gg \hbar \Gamma = \hbar (\Gamma_R + \Gamma_L + 1/\tau)$].

The transport through the quantum dot is assumed to be based on sequential single-electron hopping into and out of the quantum dot via the connected reservoirs. The energy of each electron before and after the transition must be conserved. The conserved energy includes the single-particle state energy, the charging energy against the other electrons in the quantum dot, and the electrostatic potential energy due to the applied bias across the structure. Beenakker[13] has denoted four energy balance equations for the following four tunneling processes: (1) into the quantum dot that is *initially* on the *left* (index i, L), (2) out of the quantum dot to be *finally* on the *left* (index f, L), (3) into the quantum dot that is *initially* on the *right* (index i, R), and (4) out of the quantum dot to be *finally* on the *right* (index f, R). The energy balance equations corresponding to these processes are

$$E_{p,N}^{i,L} = E_p + \tilde{U}(N+1) - \tilde{U}(N) + \eta eV \ , \quad \text{(A2a)}$$

$$E_{p,N}^{f,L} = E_p + \tilde{U}(N) - \tilde{U}(N-1) + \eta eV \ , \quad \text{(A2b)}$$

$$E_{p,N}^{i,R} = E_p + \tilde{U}(N+1) - \tilde{U}(N) - (1-\eta)eV \ , \quad \text{(A2c)}$$

$$E_{p,N}^{f,R} = E_p + \tilde{U}(N) - \tilde{U}(N-1) - (1-\eta)eV \ , \quad \text{(A2d)}$$

where N is the number of electrons in the dot *before* the tunneling event and η is the fraction of the applied voltage that drops over the left barrier (compare to Fig. 1 of Ref. 13). E_p is the single-particle eigenenergy of the quantum level p.

The usual[38,13] notation for many-electron Slater determinants is formulated in terms of Fermi particle annihilation and creation operators. Given, for example, two spin-degenerate quantum states the Slater determinants are usually denoted as $|n_{1\uparrow}, n_{1\downarrow}, n_{2\uparrow}, n_{2\downarrow}\rangle$ where the n_i can take on only values 0 and 1. For this particular example with a maximum of four fermions in a limited basis set of four states we have $2^4 = 16$ possible Slater determinants. Here we are interested in the average population of these Slater determinant states, given that they are weakly coupled to two leads. The system of equations to be solved for is of dimension 16×16. Several of these 16 states are equally occupied if the coupling to the leads is spin independent (for example, $|1,0,0,0\rangle$ and $|0,1,0,0\rangle$).

$|n_{1\uparrow},n_{1\downarrow},n_{2\uparrow},n_{2\downarrow}\rangle$ $\}\xrightarrow{cd}\{m_1 m_2\}$	
$\lvert 0\,0\,0\,0\rangle\ \}\xrightarrow{1}\{0,0\}$	$\left.\begin{array}{l}\lvert 1\,0\,1\,0\rangle\\ \lvert 1\,0\,0\,1\rangle\\ \lvert 0\,1\,1\,0\rangle\\ \lvert 0\,1\,0\,1\rangle\end{array}\right\}\xrightarrow{4}\{1,1\}$
$\left.\begin{array}{l}\lvert 1\,0\,0\,0\rangle\\ \lvert 0\,1\,0\,0\rangle\end{array}\right\}\xrightarrow{2}\{1,0\}$	
$\left.\begin{array}{l}\lvert 0\,0\,1\,0\rangle\\ \lvert 0\,0\,0\,1\rangle\end{array}\right\}\xrightarrow{2}\{0,1\}$	$\left.\begin{array}{l}\lvert 1\,1\,1\,0\rangle\\ \lvert 1\,1\,0\,1\rangle\end{array}\right\}\xrightarrow{2}\{2,1\}$
$\lvert 1\,1\,0\,0\rangle\ \}\xrightarrow{1}\{2,0\}$	$\left.\begin{array}{l}\lvert 1\,0\,1\,1\rangle\\ \lvert 0\,1\,1\,1\rangle\end{array}\right\}\xrightarrow{2}\{1,2\}$
$\lvert 0\,0\,1\,1\rangle\ \}\xrightarrow{1}\{0,2\}$	$\lvert 1\,1\,1\,1\rangle\ \}\xrightarrow{1}\{2,2\}$

FIG. 9. Example of a compression of nondegenerate to degenerate state notation. Orbitals $(n_{1\uparrow}, n_{1\downarrow})$ and $(n_{2\uparrow}, n_{2\downarrow})$ are each assumed to be spin degenerate with spin-independent coupling to the leads. The configuration $\{m_1, m_2\}$ has $m_1 = n_{1\uparrow} + n_{1\downarrow}$ and $m_2 = n_{2\uparrow} + n_{2\downarrow}$ with the configuration degeneracy $\mathcal{C}$ as indicated above the arrows. Sixteen configurations are converted to nine. We use this scheme to convert the $2^{26} = 6.7 \times 10^6$ nondegenerate configurations for 26 electrons (Fig. 3) to 8.4×10^4 configurations in the degenerate notation.

Figure 9 depicts all 16 states and groups them according to equal occupation probability. Instead of the 16 unknowns, only nine unknowns have to be calculated. We introduce notation for these nine groups, in which we simply count the number of electrons in the degenerate subgroup, as indicated in the example in Fig. 9. The nine possible configurations are now described by two numbers $\{m_1, m_2\}$, where $m_1 = n_{1\uparrow} + n_{1\downarrow}$ and $m_2 = n_{2\uparrow} + n_{2\downarrow}$. Each "state" m_1 and m_2 is twofold degenerate and its index can take on values 0, 1, and 2.

While the reduction from 16 to 9 configurations does not appear significant, larger systems show a dramatic reduction. Including lateral state degeneracies [see Fig. 3(b)] as well as the spin degeneracies (see Fig. 9) we can compress our system to five fourfold and three twofold degenerate groups. We denote the degeneracy of each state as d_p and the index m_p can take on values $\{0, \ldots, d_p\}$. We reduce our system from $2^{26} = 67,108,864$ to $\prod_{p=1}^{N_{\text{group}}} (d_p + 1) = 5^5 \times 3^3 = 84\,375$ ($N_{\text{group}} = 8$ in our case; see Fig. 3), which is a reduction by a factor of about 800. To keep track of the multiple degeneracies we have introduced the configuration degeneracy $\mathcal{D}$, as indicated in Fig. 9. In the example in Fig. 9 the configuration degeneracy takes on values 1, 2, and 4, depending on the configuration $\{m_1, m_2\}$. The configuration degeneracy $\mathcal{D}\{m_1, m_2, \ldots, m_{N_{\text{group}}}\}$ can be formally defined as a product of binomial coefficients ${}^{d_p}C_{m_p} = \frac{d_p!}{m_p!(d_p - m_p)!}$:

$$\mathcal{D}(\{m_k\}) = \prod_{p=1}^{N_{\text{group}}} {}^{d_p}C_{m_p} \ , \tag{A3}$$

where we use the short form $\{m_k\} = \{m_1, m_2, \ldots, m_p, \ldots, m_{N_{\text{group}}}\}$ and $m_p \in \{0, \cdots, d_p\}$.

Given the probability of occupation of each configuration $P(\{m_k\})$ and a Fermi-Dirac distribution in the reservoirs of $f(E) = \left[1 + \exp\left(\frac{E - E_F}{k_B T}\right)\right]^{-1}$, the steady state current through the left barrier (which equals the current through the right barrier) is given by

$$I = -e \sum_{\{m_k\}} \mathcal{D}(\{m_k\})\ P(\{m_k\}) \sum_{p=1}^{N_{\text{group}}} (d_p - m_p)\, \Gamma_{p,N}^{i,L}\, f_{p,N}^{i,L} - m_p \Gamma_{p,N}^{f,L}\left(1 - f_{p,N}^{f,L}\right)\ , \tag{A4}$$

where m_p is the number of electrons in group p and N_{group} is the number of quantum levels considered. The tunneling rate Γ and lead state occupation probability f carry four indices indicating the energy dependence of the transition as indicated in Eq. (A2). The index p on Γ is also used to keep track of the lateral mode dependent, i.e., state dependent, coupling to the subbands in the leads.

The rate equations for the nonequilibrium occupation probability $P(\{m_i\})$ including the degeneracy read

$$0 = \frac{\partial}{\partial t} P(\{m_k\}) = -\sum_p P(\{m_k\})\ (d_p - m_p)\ \left\{\Gamma_{p,N}^{i,L} f_{p,N}^{i,L} + \Gamma_{p,N}^{i,R} f_{p,N}^{i,R}\right\}$$

$$- \sum_p P(\{m_k\})\ m_p\ \left\{\Gamma_{p,N}^{f,L}\left[1 - f_{p,N}^{f,L}\right] + \Gamma_{p,N}^{f,R}\left[1 - f_{p,N}^{f,R}\right]\right\}$$

$$+ \sum_p P(\ldots, m_{p-1}, m_p + 1, m_{p+1}, \ldots)\ (d_p - m_p)\ \left\{\Gamma_{p,N+1}^{f,L}\left[1 - f_{p,N+1}^{f,L}\right] + \Gamma_{p,N+1}^{f,R}\left[1 - f_{p,N+1}^{f,R}\right]\right\}$$

$$+ \sum_p P(\ldots, m_{p-1}, m_p - 1, m_{p+1}, \ldots)\ m_p\ \left\{\Gamma_{p,N-1}^{i,L} f_{p,N-1}^{i,L} + \Gamma_{p,N-1}^{i,R} f_{p,N-1}^{i,R}\right\}$$

$$- \mathcal{D}(\{m_k\})\ \frac{P(\{m_k\}) - P_0(\{m_k\})}{\tau}\ , \quad \forall\, \{m_k\}. \tag{A5}$$

We have argued in Sec. II A that each state $\{m_k\}$ with n electrons is connected to other states by five basic processes and we repeat them here for the more general case: (1) destruction of $\{m_k\}$ by inflow of electrons, (2) destruction of $\{m_k\}$ by outflow of electrons, (3) creation of $\{m_k\}$ by destruction of a state with $(n+1)$ electrons, (4)

creation of $\{m_k\}$ by destruction of a state with $(n-1)$ electrons, and (5) destruction of $\{m_k\}$ due to relaxation. These five processes are reflected in that order in the five contributions in Eq. (A5). The set of equations (A5) contains $\prod_{p=1}^{N_{\text{group}}} (d_p + 1)$ equations for the same number of unknowns. However, one of the equations is a linear com-

bination of the others and the system is underdetermined by one equation. The normalization of the probabilities to 1 closes the system:

$$\sum_{\{m_k\}} \mathcal{D}(\{m_k\}) \; P(\{m_k\}) = 1 \; . \qquad (A6)$$

Equation (A5) is equivalent to Eq. (2.12) in Ref. 13 except for the phenomenological intra quantum dot relaxation and the degenerate state notation. The canonical probability distribution $P_0(\{m_k\})$ depends on the free energy of the internal degrees of freedom with a fixed number of electrons in the quantum dot and the probability to have that particular number:

$$P_0(\{m_k\}) = \frac{\mathcal{D}(\{m_k\}) \; \exp\left(\sum_{p=1}^{\infty} E_p m_p \Big/ k_B T\right)}{\sum_{\{o_k\}} \mathcal{D}(\{o_k\}) \; \exp\left(\sum_{p=1}^{\infty} E_p o_p \Big/ k_B T\right) \delta_{N,\sum_p o_p}} \; P(N) \; . \qquad (A7)$$

The probability $P(N)$ represents the probability to have a total number N electrons in the quantum dot regardless of electron configuration. It is the sum of all configurations with the total number of N electrons:

$$P(N) = \sum_{\{m_k\}} \mathcal{D}(\{m_k\}) \; P(\{m_k\}) \; \delta_{N,\sum_p m_p} \; . \qquad (A8)$$

The introduction of the relaxation rate couples all configurations with the same total number of electrons N with each other, since $P_0(\{m_k\})$ depends now on all configurations with N electrons.

In order to solve this large system of equations iteratively[33] we need to find a "good" guess for a fast solution. We obtain our guess for the most likely configuration by looking at the diagonal elements of the matrix. The diagonal elements indicate the leakage of the corresponding configuration to other configurations. The configuration with the smallest leakage rate to other configurations is the most stable one and will be the most likely one to occur. We use this physical argument to justify our initial guess of the probability distribution and achieve satisfactory convergence in the iterative procedure.

2. Strong inelastic scattering

Beenakker[13] has given equations for the nonequilibrium number of electrons in the quantum dot similar to

Averin et al.[14] We continue to use the same notation and extend Beenakker's[13] Eq. (5.1) to multiple degeneracy. The modified equation of detailed balance reads now

$$P(N+1) \, \Gamma^{\text{out}}(N+1) = P(N) \, \Gamma^{\text{in}}(N) \; , \qquad (A9)$$

with

$$\begin{aligned} \Gamma^{\text{out}}(N+1) = \sum_{p=1}^{N_{\text{group}}} & F_{\text{eq}}(E_p|N+1) \\ & \times \left\{ \Gamma^{f,L}_{p,N+1} \left[1 - f^{f,L}_{p,N+1}\right] \right. \\ & \left. + \Gamma^{f,R}_{p,N+1} \left[1 - f^{f,R}_{p,N+1}\right] \right\} \; , \end{aligned} \qquad (A10)$$

$$\begin{aligned} \Gamma^{\text{in}}(N) = \sum_{p=1}^{N_{\text{group}}} & [d_p - F_{\text{eq}}(E_p|N)] \\ & \times \left[\Gamma^{i,L}_{p,N} f^{i,L}_{p,N} + \Gamma^{i,R}_{p,N} f^{i,R}_{p,N} \right] \; , \end{aligned} \qquad (A11)$$

where $F_{\text{eq}}(E_p|N)$, the equilibrium probability of finding state p occupied, given that N electrons are in the quantum dot, is defined as

$$F_{\text{eq}}(E_p|N) = \frac{\displaystyle\sum_{\{m_k\}} \delta_{N,\sum_i m_i} \left(1 - \delta_{m_p,0}\right) \mathcal{D}(\{m_k\}) \; \exp\left(\sum_{i=1}^{N_{\text{group}}} E_i m_i \Big/ k_B T\right)}{\displaystyle\sum_{\{m_k\}} \delta_{N,\sum_i m_i} \mathcal{D}(\{m_k\}) \; \exp\left(\sum_{i=1}^{N_{\text{group}}} E_i m_i \Big/ k_B T\right)} \; . \qquad (A12)$$

The set of N equations (A9) for $N+1$ unknowns is closed by the normalization condition:

$$\sum_{N=0}^{N_{\text{total}}} P(N) = 1 \; . \qquad (A13)$$

After solving for $P(N)$ with Eqs. (A9) and (A13) we use Eq. (A7) to determine $P(\{m_k\})$ with the assumption of thermalization $[P(\{m_k\}) = P_0(\{m_k\})]$ and evaluate the current through the structure using Eq. (A4).

Equation (A9) can be interpreted as a recursive relation[14] determining the filling of a $(N+1)$-electron

state based on the realization of an N-electron state: $P(N{+}1)=\frac{P(N)\Gamma^{in}(N)}{\Gamma^{out}(N{+}1)}$. If $\Gamma^{in}(N=0)=0$ then $P(N=1)=0$ and all subsequent $P(N>1)=0$. The in-tunneling rate $\Gamma^{in}(N=0)$ is indeed zero if all single-particle states are pulled under the emitter conduction band (see the inset in Fig. 4 or 5). Consequently the current transport through the quantum dot shuts off at the same bias as if there were no charging [see Figs. 5 and 7(a)] and the average number of electrons in the quantum dot $\langle N \rangle$ changes abruptly from a finite value to zero.

If each bias point in a I-V characteristic is considered to be a perturbation of an infinitesimal smaller bias point, then the average number of electrons in the quantum dot could be expected to change only infinitesimally. If another boundary condition for the average number of electrons $\langle N \rangle \neq 0$ is introduced into the system of equations, then the system becomes overdetermined in the case of $\Gamma^{in}(N)=0$ and $\Gamma^{in}(N+1)\neq 0$ for any N. The recursive Eq. (A9) could be thought of as being solved from large values of N down to smaller values of N: $P(N)=\frac{P(N{+}1)\Gamma^{out}(N{+}1)}{\Gamma^{in}(N)}$. Equations involving $\Gamma^{in}(N)=0$ cause the recursive chain to end and the associated probabilities $P(N)$ are ill defined. If these probabilities $P(N)$ are set to zero, a second bistable solution with $\langle N \rangle \neq 0$ can be found.

Effects of bistability have been discussed by Averin et al.[14] We have included possible bistability into our model in the scheme discussed in the preceding paragraph and found that the inclusion of subband mixing washes out effects due to bistability in the voltage range discussed in this paper. This is due to the effect that $\Gamma^{in}(N=1)\neq 0$ even for high biases, since the single-particle levels are not decoupled until the highest single-particle state is pulled under the emitter conduction band edge. This bias range would be even increased further if optical phonon scattering would be included as discussed in Refs. 29 and 30. We do not include our results on bistability here since they have been discussed by Averin et al.[14] in detail already.

3. Constant charging interaction

Several calculations of the many-body eigenenergies of quantum dots have been performed.[22-27,39,41] The critical ingredient in these calculations is the form of the electron-electron interaction potential and the cited references differ in their choices of this potential. Many-body spectra using the unscreened[22,23] Coulomb potential $\frac{1}{|\vec{r}_i-\vec{r}_j|}$ were analyzed first and strong spatial electron-electron correlations were found in the case of comparable interaction energy and single-electron quantum state spacing. The many-body ground state has significant contributions of excited single-particle states indicating how electrons arrange themselves spatially to reduce the charging energy in this limit. Häusler and Kramer[26] have used an interaction potential of the form $\frac{1}{(|x_i-x_j|^2+\lambda^2)^{1/2}}$ in their quasi-one-dimensional calculation and pointed out limitations of the state independent charging model. Johnson and Payne[24,39] introduced a modified interac-

tion potential of parabolic form which mimics the saturation of the interation potential for small distances. The problem becomes exactly solvable and its results have been shown to be comparable[25] to the Coulomb potential interaction in the limit of strong confinement.

The purpose of this section is to relate the state independent charging energy to a microscopic calculations. Starting from there we argue[42] similar to a discussion in Ref. 22 that the simple charging model may give reasonable results for structures in which the single-particle quantization energy is the dominant energy scale. Figure 10 depicts[39] the forms of the three investigated electron-electron potentials: Coulomb, modified Coulomb, and parabolic potential. If the region of confinement is small and screening by spatially closely located ground planes is reasonable to assume, then a constant interaction potential as indicated by a horizontal line in Fig. 10 may be a reasonable assumption.

Starting with the definitions of one- and two-electron integrals over spin and spatial orbitals in Ref. 38 on p. 68, we substitute the two-electron operator r_{ij}^{-1} by a spatially independent constant U and calculate the N-particle Hamiltonian matrix on the basis set of N-particle Slater determinants. The choice of orthonormal single-particle basis set for the generation of the N-particle Slater determinants and the spatially independent electron-electron interaction potential allows an easy analytic calculation of the Hamiltonian matrix elements. The Hamiltonian matrix turns out to be diagonal and with an expression for a N-particle Slater determinant denoted in configuration space as $\{n_i\}=\{n_1,n_2,\ldots,n_p\}$ we obtain, for the diagonal elements,

$$E_{\{n_i\}}=\sum_i E_i\delta_{n_i,1}+\frac{U}{2}N(N-1),\qquad (A14)$$

where E_i is the single-particle eigenenergy of the ith spin orbital and $N=\sum_{i=1}^p n_i$. This approach allows a natural derivation of the charging energy expression [Eq. (A1)] which we are using in this work. The charging energy of single electrons against image charges in surrounding ground planes is not considered here.[40]

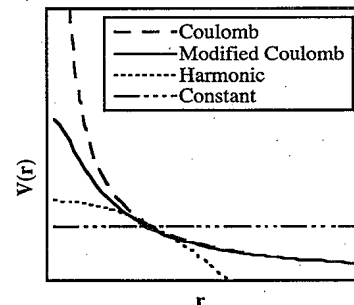For our numerical simulations we chose the device pa-

FIG. 10. Electron-electron charge interaction potentials $V(r)$. Coulomb, modified Coulomb, harmonic, and constant potential.

rameters such that the single-particle energy separation ΔE is larger than the charging energy U. This is the parameter region in which the constant charging interaction model is still valid.[22] In general we could implement a given many-body spectrum with all its ground states and excitations into the rate equation approach

used here. However, we feel that at this stage detailed calculations of state spectra will not improve our discussion of the general trends discussed in this paper. Also the confinement potentials and interaction potentials are not known accurately[42] enough to justify more detailed calculations.

* Present address: Eric Jonsson School of Engineering and Computer Science, University of Texas at Dallas, Richardson, TX 75083-0688.

† Present address: Central Research Laboratory, Texas Instruments, Inc., Dallas, TX 75265.

[1] F. Capasso, MRS Bull. **16**, 23 (1991).

[2] F. Capasso, K. Mohammed, and A. Y. Cho, IEEE J. Quantum Electron. **QE-22**, 1853 (1986).

[3] S. Datta and M. J. McLennan, Rep. Prog. Phys. **53**, 1003 (1990).

[4] V. J. Goldman, D. C. Tsui, and J. E. Cunningham, Phys. Rev. Lett. **58**, 1256 (1987).

[5] F. W. Sheard and G. A. Toombs, Appl. Phys. Lett. **52**, 1228 (1988).

[6] *Resonant Tunneling in Semiconductor Physics and Applications*, edited by L. L. Chang, E. E. Mendez, and C. Tejedor (Plenum, New York, 1991).

[7] R. Lake, G. Klimeck, and S. Datta, Phys. Rev. B **47**, 6427 (1993), and references therein.

[8] B. Su, J. V. Goldman, and J. E. Cunningham, Phys. Rev. B **46**, 7644 (1992).

[9] M. Tewordt et al., Phys. Rev. B. **45**, 14 407 (1992).

[10] M. A. Reed et al., Phys. Rev. Lett. **60**, 535 (1988).

[11] S. Tarucha, Y. Hirayama, and Y. Tokura, Appl. Phys. Lett. **58**, 1623 (1991).

[12] B. Su, J. V. Goldman, M. Santos, and M. Shayegan, Appl. Phys. Lett. **58**, 747 (1991).

[13] C. W. J. Beenakker, Phys. Rev. B **44**, 1646 (1991).

[14] D. V. Averin, A. N. Korotkov, and K. K. Likharev, Phys. Rev. B **44**, 6199 (1991).

[15] G. W. Bryant, Phys. Rev. B **39**, 3145 (1989).

[16] G. W. Bryant, Phys. Rev. B **44**, 3782 (1991).

[17] G. W. Bryant, Phys. Rev. B **44**, 12 837 (1991).

[18] H. C. Liu and G. C. Aers, J. Appl. Phys. **65**, 4908 (1989).

[19] T. Inoshita and H. Sakaki, Phys. Rev. B **46**, 7260 (1992).

[20] We have also considered (see Ref. 21) finite relaxation rates in a simple two state model. We can show with analytical results, including a finite relaxation rate $1/\tau$, how the limit of $\tau \to 0$ converges to the thermalization result by Averin et al. (Ref. 14). For the numerical treatment we only consider the two limiting cases of rapid thermalization (strong inelastic scattering) and elastic transport.

[21] G. Klimeck, Ph.D. thesis, Purdue University, School of Electrical Engineering, 1994.

[22] G. W. Bryant, Phys. Rev. Lett. **59**, 1140 (1987).

[23] P. A. Maksym and T. Chakraborty, Phys. Rev. Lett. **65**, 108 (1990).

[24] N. F. Johnson and M. C. Payne, Phys. Rev. B **45**, 3819 (1992).

[25] B. L. Johnson and G. Kirczenow, Phys. Rev. B **47**, 10 563 (1993).

[26] W. Häusler and B. Kramer, Phys. Rev. B **47**, 16 353 (1993).

[27] A. Kumar, S. E. Laux, and F. Stern, Phys. Rev. B **42**, 5166 (1990).

[28] G. W. Bryant, Phys. Rev. B **44**, 3064 (1991).

[29] R. Lake, G. Klimeck, and S. Datta, Phys. Rev. B **47**, 6427 (1993).

[30] R. Lake, G. Klimeck, M. P. Anantram, and S. Datta, Phys. Rev. B **48**, 15 132 (1993).

[31] If we were to include all states depicted in Fig. 3(a) we would obtain six fourfold and four twofold degenerate states with a dimension, of the configuration space of $5^6 \times 3^4 = 1,265,625$. A coupled system of equations of this dimension is not treatable with reasonable computation times anymore.

[32] Since we are leaving out the states $\{(1,3);(3,1)\}$ and $\{(3,3)\}$, we are leaving out additional fine structure in the I-V characteristic. However, the qualitative features of sharp mode turnons and turnoffs will still exist in the full solution.

[33] T. C. Oppe, W. D. Joubert, and D. R. Kincaid (unpublished).

[34] G. Klimeck, R. K. Lake, M. J. McLennan, and S. Datta (unpublished).

[35] S. Adachi, J. Appl. Phys. **58**, R1 (1985).

[36] Lateral states 3 and 4 are degenerate (see Fig. 3) and we can assume them to be *one* state in this discussion.

[37] The first and second levels [$1\hbar\omega$ and $2\hbar\omega$ in Fig. 3(b)] combined can hold six electrons. The third single-particle level [$3\hbar\omega$ in Fig. 3(b)] can hold six electrons. However, the bias necessary to fill in the seventh electron is beyond the turnoff of all the single-particle levels and no explicit turnon of level 3 can be found in the I-V characteristic. If the effect of bistability would be included here, we could obtain a bistable turnon of level 3. See the discussion including bistability in the Appendix following Eq. (A9).

[38] A. Szabo and N. S. Ostlund, *Modern Quantum Chemistry: Introduction to Advanced Electronic Structure Theory* (Macmillan, New York, 1982).

[39] N. F. Johnson and M. C. Payne, Superlatt. Microstruct. **11**, 309 (1992).

[40] L. Y. Chen and C. S. Ting, Phys. Rev. B **44**, 5916 (1991).

[41] Gerhard Klimeck, Guanlong Chen, and Supriyo Datta, Phys. Rev. B **50**, 2316 (1994).

[42] Reference 41 compares interaction energies for the models of Coulomb interaction $1/|r_i - r_j|$, modified Coulomb interaction $1/(|r_i - r_j|^2 + \lambda^2)^{1/2}$, and screened Coulomb interaction $\exp(-|r_i - r_j|/\beta)/|r_i - r_j|$ and indicates the strong model dependence of the associated charging energies.

[43] D. V. Averin and A. N. Korotkov, Sov. Phys. JETP **70**, 937 (1990).